HHS Public Access

Author manuscript

Biomaterials. Author manuscript; available in PMC 2016 June 01.

Published in final edited form as:

Biomaterials. 2015 June ; 53: 149–159. doi:10.1016/j.biomaterials.2015.02.092.

Acellular Bi-Layer Silk Fibroin Scaffolds Support Functional Tissue Regeneration in a Rat Model of Onlay Esophagoplasty

Khalid Algarrahi[1,2], **Debra Franck**[1], **Chiara Ghezzi**[3], **Vivian Cristofaro**[2,4,5], **Xuehui Yang**[1], **Maryrose P. Sullivan**[2,4,5], **Yeun Goo Chung**[1,2], **Saif Affas**[1,2], **Russell Jennings**[2], **David L. Kaplan**[3], **Carlos R. Estrada Jr.**[1,2,§], and **Joshua R. Mauney**[1,2,§]

[1]Urological Diseases Research Center, Boston Children's Hospital, Boston, MA 02115, USA

[2]Department of Surgery, Harvard Medical School, Boston, MA 02115, USA

[3]Department of Biomedical Engineering, Tufts University, Medford, MA, 02155, USA

[4]Division of Urology, Veterans Administration Boston Healthcare System, West Roxbury, MA 02132, USA

[5]Department of Surgery, Brigham and Women's Hospital, Boston, MA 02115, USA

Abstract

Surgical management of long-gap esophageal defects with autologous gastrointestinal tissues is frequently associated with adverse complications including organ dysmotility, dysphagia, and donor site morbidity. In order to develop alternative graft options, bi-layer silk fibroin (SF) scaffolds were investigated for their potential to support functional tissue regeneration in a rodent model of esophageal repair. Onlay esophagoplasty was performed with SF matrices (N=40) in adult rats for up to 2 m of implantation. Parallel groups consisted of animals implanted with small intestinal submucosa (SIS) scaffolds (N=22) or sham controls receiving esophagotomy alone (N=20). Sham controls exhibited a 100% survival rate while rats implanted with SF and SIS scaffolds displayed respective survival rates of 93% and 91% prior to scheduled euthanasia. Animals in each experimental group were capable of solid food consumption following a 3 d post-op liquid diet and demonstrated similar degrees of weight gain throughout the study period. End-point μ-computed tomography at 2 m post-op revealed no evidence of contrast extravasation, fistulas, strictures, or diverticula in any of the implant groups. Ex vivo tissue bath studies demonstrated that reconstructed esophageal conduits supported by both SF and SIS scaffolds displayed contractile responses to carbachol, KCl and electrical field stimulation while isoproterenol produced tissue relaxation. Histological (Masson's trichrome and hematoxylin and eosin) and immunohistochemical (IHC) evaluations demonstrated both implant groups produced

[§]Corresponding authors: Joshua R. Mauney, Ph.D., Boston Children's Hospital, Department of Urology, John F. Enders Research Laboratories, 300 Longwood Ave., Rm. 1009, Boston, MA 02115, USA; Phone: 617-919-2521; Fax: 617-730-0248; joshua.mauney@childrens.harvard.edu; Carlos Estrada, M.D., Boston Children's Hospital, Department of Urology, 300 Longwood Ave., Hunnewell 3, Boston, MA 02115, USA; Phone: 617-355-3338; Fax: 617-730-0474; carlos.estrada@childrens.harvard.edu.

de novo formation of skeletal and smooth muscle bundles positive for contractile protein expression [fast myosin heavy chain (MY32) and α-smooth muscle actin (α-SMA)] within the graft site. However, SF matrices promoted a significant 4-fold increase in MY32+ skeletal muscle and a 2-fold gain in α-SMA+ smooth muscle in comparison to the SIS cohort as determined by histomorphometric analyses. A stratified squamous, keratinized epithelium expressing cytokeratin 5 and involucrin proteins was also present at 2 m post-op in all experimental groups. De novo innervation and vascularization were evident in all regenerated tissues indicated by the presence of synaptophysin (SYP38)+ boutons and vessels lined with CD31 expressing endothelial cells. In respect to SIS, the SF group supported a significant 4-fold increase in the density of SYP38+ boutons within the implant region. Evaluation of host tissue responses revealed that SIS matrices elicited chronic inflammatory reactions and severe fibrosis throughout the neotissues, in contrast to SF scaffolds. The results of this study demonstrate that bi-layer SF scaffolds represent promising biomaterials for onlay esophagoplasty, capable of producing superior regenerative outcomes in comparison to conventional SIS scaffolds.

Keywords

silk; scaffold; wound healing; muscle; epithelium

1. Introduction

The esophagus is a tubular, fibromuscular organ responsible for the transport of food from the pharynx to the stomach via peristaltic contractions. Long-gap esophageal defects resulting from congenital abnormalities such as esophageal atresia and tracheoesophageal fistula as well as acquired diseases including Barrett's esophagus, gastroesophageal reflux, squamous cell carcinoma, and strictures are often repaired with gastric pull-up or interposition grafts using either jejunum or colon to restore organ continuity [1–4]. Unfortunately, these approaches are associated with severe adverse complications such as esophageal dysmotility and dysphagia as well as donor site morbidity, all of which can severely impair patient quality of life [5–7]. Therefore, there exists a significant need for the development of alternative methods for esophageal tissue reconstruction.

Tissue engineering strategies deploying 3-D biodegradable scaffolds either alone or seeded with primary or multi-potent cell sources have been investigated for esophageal tissue replacement [8–11]. Cell-free grafts derived from extracellular matrices (ECM) such as decellularized esophagus [12], decellularized urinary bladder submucosa (UBS) [13], acellular dermis [14], gastric acellular matrix [15], small intestinal submucosa (SIS) [16–19], decellularized aorta [20] and collagen-based sponges [21–24] have been shown to promote host tissue ingrowth and constructive tissue remodeling in a number of animal models of esophageal reconstruction. In addition, small-scale clinical trials have also demonstrated the feasibility of SIS and UBS implants for the repair of esophageal defects [25–27]. However, deleterious side-effects including graft contracture, implant perforation, stenosis, and stricture formation have been frequently reported with the use of these ECM-derived matrices for esophagoplasty [16, 17, 24, 26, 28], thus raising concerns over their wide-scale translational potential. Synthetic polyester-based matrices either alone [29] or

seeded with primary esophageal organoid units [30] or oral keratinocytes and fibroblasts [31] have also been shown to encourage regeneration of esophageal defects in preclinical studies. The degradation metabolites of polyesters, however, are known to elicit chronic inflammatory responses in vivo [32] and therefore have the potential to negatively impact long-term organ function due to adverse foreign body reactions [33]. Given the limitations associated with conventional implant designs, new options for esophageal tissue engineering must be explored.

Bi-layer silk fibroin (SF) matrices derived from *Bombyx mori* silkworm cocoons represent acellular, biodegradable implants which are specifically designed to facilitate repair of hollow organ defects [34, 35]. The unique bi-layer scaffold configuration is composed of a porous SF foam which allows for ingrowth of surrounding host tissues, while an annealed SF film functions to provide a fluid-tight seal for retention of hollow organ contents during defect consolidation [34, 35]. In vitro biocompatibility studies have shown the propensity of these biomaterials to support attachment, proliferation, and differentiation of esophageal cell lines; key cellular processes involved in promoting host tissue integration and functional maturation of regenerating tissue [36]. Previous reports from our group have demonstrated the utility of bi-layer SF scaffolds to promote constructive tissue remodeling within the urinary bladder [34, 35, 37] and the urethra [38], however their potential for esophageal tissue repair is unknown. In the present study, we investigated the efficacy of these scaffolds to support functional tissue regeneration in a rat model of onlay esophagoplasty.

2. Materials and Methods

2.1. Biomaterials

Aqueous SF solutions were prepared from *B. mori* silkworm cocoons and utilized to construct a bi-layer SF matrix using methods previously described [34, 39]. Briefly, a SF solution (8% wt/vol) was poured into a rectangular casting vessel and dried in a laminar flow hood at room temperature for 48 h to achieve formation of a SF film. A 6% wt/vol SF solution was then mixed with sieved granular NaCl (500–600 μm, average crystal size) in a ratio of 2 g NaCl per ml of SF solution and layered on to the surface of the SF film. The resultant solution was allowed to cast and fuse to the SF film for 48 h at 37°C and NaCl was subsequently removed by washin g the scaffold for 72 h in distilled water with regular volume changes. The morphology of the bi-layer SF scaffold has been previously reported [34]. Briefly, the solvent-cast/NaCl-leached layer comprised the bulk of the total matrix thickness (2 mm) and resembled a foam configuration with large pores (pore size, ~400 μm) interconnected by a network of smaller pores dispersed along their periphery. This compartment was buttressed on the external face with a homogenous, non porous SF layer (200 μm thick) generated by film annealing during casting. Prior to implantation, bi-layer SF scaffolds were sterilized in 70% ethanol and rinsed in phosphate buffered saline (PBS) overnight. SIS matrices (Cook, Bloomington, IN) were evaluated in parallel as a standard point of comparison. Tensile properties of both scaffold configurations have been previously reported [34].

2.2. Onlay esophagoplasty rat model

Scaffold groups (SF: N=40; SIS: N=22) were evaluated in an onlay esophagoplasty model (Figure 1A, B) using female Sprague-Dawley rats (6–8 wks of age, ~140–200 g, Charles River Laboratories, Wilmington, MA). Prior to surgery, animals were maintained for 24 h on a liquid diet consisting of a nutritionally-balanced commercial formula (TestDiet®, Richmond, IN mixed with PediaSure®, Abbott Laboratories, Columbus, OH) and were given ready access to water. Under general anesthesia induced by isoflurane inhalation, an upper midline laparotomy incision was made through the skin and underlying rectus muscle in a sterile fashion. The peritoneum was entered, the abdominal esophagus was exposed using blunt dissection and held in place using two vessel loops. A 7×3 mm^2 elliptical defect was created in the anterior esophageal wall 5 mm above the gastroesophageal junction via surgical tissue resection. An elliptical graft of equal size was incorporated into the defect site using interrupted 7-0 polyglactin sutures. Non-absorbable 7-0 polypropylene sutures were placed at the proximal/distal and lateral edges of the anastomotic perimeter for identification of graft borders. A sham-operated control group of animals (N=20) receiving esophagotomy alone were treated similarly in parallel. Following these procedures, the esophagus was replaced into the abdominal cavity, covered with omentum, and the skin and abdominal incisions were sutured closed. Post-operative pain was managed with meloxicam (1 mg/kg, subcutaneously) and buprenorphine (0.1 mg/kg, subcutaneously). All animals were maintained on the liquid diet described above for 3 d post-op and subsequently transferred to standard rat chow for the duration of the study. Animals were weighed prior to surgery and every week until scheduled euthanasia. Rats receiving SF implants were harvested for endpoint evaluations at 1 d (N=3), 1 wk (N=3), 1 m (N=11), and 2 m (N=20) post-op. Sham-operated controls (N=20) and animals implanted with SIS scaffolds (N=20) were harvested at 2 m following surgical manipulation. An additional group of non-surgical (NS) control rats (N=4) were euthanized in parallel for endpoint comparisons. All animal studies were approved by the Boston Children's Hospital Animal Care and Use Committee prior to experimentation.

2.3. Micro-computed tomography (μCT) imaging

MicroCT analysis was performed on control and implant groups (N=8–9 per group) at 2 m postop utilizing a high resolution Albira preclinical PET/SPECT/CT system (Bruker Corporation, Billerica, MA) to evaluate esophageal continuity and the presence of strictures or organ dilation. Animals were anesthetized by isoflurane inhalation and gavaged with contrast agent (Varibar® Pudding Barium Sulfate Esophageal Paste) into the proximal esophagus. Axial images of the entire esophagus were acquired (45 kV, 400 μA, 600 projections, 125 μm voxel resolution) following contrast agent gavage and sagittal, coronal and 3D views were reconstructed using Albira software suite (version 5.0, Bruker Corporation). Luminal esophageal cross-sectional areas were then quantified from the central regions of the original scaffold implantation sites or control esophagotomy as well as a reference point adjacent to the 7^{th} thoracic vertebra (T7) using Volview (version 3.4, http://www.kitware.com/) and ImageJ (version 1.47, http://imagej.nih.gov/ij/) software.

2.4. Mechanical testing

Uniaxial tensile tests were performed on experimental groups (N=4–5 per group) at 2 m postop with a Dynamic Mechanical Analyzer (TA Instruments, New Castle, DE) equipped with a 10 N capacity load cell and hand-tightening mechanical grips. Rectangular esophageal specimens (~48 mm^2) containing the original graft site or control tissue were hydrated in PBS at 37°C before testing and were kept hydrated throughout the entire testing period. A displacement control mode with a crosshead displacement rate of 0.3 mm/s was used, and the gauge length was ~5 mm. The initial elastic modulus (EM), ultimate tensile strength (UTS) and % elongation to failure (ETF) were calculated from stress/strain plots. EM was calculated by using a least-squares (LS) fitting between 0.02 N load and 5% strain past this initial load point. UTS was determined as the highest stress value attained during the test. ETF was determined from the last strain data point before a >10% decrease in the load was encountered during testing. Percent original length was calculated as the % change in axial length of the specimen following loading relative to the pre-load value.

2.5. Ex vivo contractility and relaxation

Esophageal tissue from both scaffold groups and sham-operated controls were subjected to ex vivo contractility and relaxation analyses at 2 m post-op as previously described [35, 40]. Circular esophageal rings with intact mucosa (N=5 per group) were prepared from tubular segments containing the original scaffold implantation site and adjacent host esophageal wall. Esophageal rings were suspended in tissue baths containing Kreb's solution [NaCl 120 mM; KCl 5.9 mM; $NaHCO_3$ 25 mM; $Na_2H_2PO_4$ 1.2 mM; MgCl • 6H2O 1.2 mM; $CaCl_2$ 2.5 mM; dextrose 11.5 mM) and attached to an isometric force transducer (Grass Technologies, Warwick, RI). Tissue baths were maintained at 37°C and bubbled continuously with a mixture of 95% O_2 and 5% CO_2. After applying a pre-load of 0.5 g, tissue rings were equilibrated for 1 hour. Contractile responses were induced by exposure to KCl (80 mM) and to electrical field stimulation (EFS, 40 V, 0.5 ms pulse width, 2–25 Hz; 2 seconds duration). Relaxation responses were induced by administration of isoproterenol (10 μM) to tissues pre-contrated with carbachol (1 μM). Force measurements were digitally acquired at 30 Hz (DI-720 data acquisition system, DataQ Instruments) and continuously recorded using WinDaq Software. The amplitude of esophageal contraction was expressed as force (mN) normalized by tissue cross-sectional area. Relaxation responses were expressed as percent change from pre-contracted status.

2.6. Histological, immunohistochemical, and histomorphometric analyses

Following scheduled euthanasia, tubular esophageal segments from experimental groups were excised for standard histological processing. Briefly, specimens were fixed in 10% neutral-buffered formalin, dehydrated in graded alcohols, and then embedded in paraffin. Sections (5 μm) were cut and then stained with hematoxylin and eosin (H&E) or Masson's trichrome (MTS) using routine histological protocols. For immunohistochemical (IHC) analyses, the contractile skeletal muscle marker, fast myosin skeletal heavy chain (MY32); the contractile smooth muscle maker, α-smooth muscle actin (α-SMA); epithelial-associated proteins, pan-cytokeratin (CK), CK5, involucrin (IVL); neuronal and endothelial markers, synaptophysin (SYP38) and CD31, respectively, and the proliferation marker, Ki67 were

detected using the following primary antibodies: anti-MY32 [Abcam, Cambridge, MA, 1:200 dilution], anti-α-SMA [Sigma-Aldrich, St. Louis, MO, 1:200 dilution], anti-pan-CK [Dako, Carpinteria, CA, 1:150 dilution], anti-CK5 [Abcam, 1:200 dilution], anti-IVL [Sigma-Aldrich, 1:200 dilution], anti-SYP38 [Abcam, 1:50 dilution], anti-CD31 [Abcam, 1:100 dilution], and anti-Ki67 [Abcam, 1:200 dilution]. Sections were then incubated with species-matched Cy3 or FITC-conjugated secondary antibodies (Millipore, Billerica, MA) and nuclei were counterstained with 4', 6-diamidino-2-phenyllindole (DAPI). Specimens were visualized using an Axioplan-2 microscope (Carl Zeiss MicroImaging, Thornwood, NY) and representative images were acquired using Axiovision software (version 4.8).

Histomorphometric analyses (N=3–11 animals per group) were performed as previously described [37, 38] to assess the degree of constructive tissue remodeling in both control and implant groups using ImageJ software (version 1.47). Image thresholding and area measurements were carried out on 8 independent microscopic fields (magnification 20X) equally dispersed along the periphery and central regions of the original surgical sites to determine the percentage of stained tissue area occupied by MY32+ skeletal muscle bundles, α-SMA+ smooth muscle bundles and CK+ epithelia relative to the total field area examined. The number and diameter of CD31+ vessels and SYP38+boutons were measured similarly in 4–8 independent microscopic fields (magnification 20X) and normalized to the total field area examined to ascertain the respective extent of *de novo* vascularization and innervation processes in all experimental groups. In addition, the percentage of Ki67+ cells per total cell population examined was also quantified in 3 independent microscopic fields to determine the extent of cell proliferation.

2.7. Statistical analysis

Quantitative measurements were analyzed with the Kruskal-Wallis test in combination with the post-hoc Scheffé's method. All statistical evaluations were performed with SPSS Statistics software v19.0 (http://www.spss.com) and all data were expressed as means ± standard deviation. Statistically significant values were defined as $p<0.05$.

3. Results and Discussion

Prior to scheduled euthanasia, animals implanted with SF and SIS scaffolds displayed respective survival rates of 93% (37/40) and 91% (20/22) in comparison to a 100% survival rate for sham controls (20/20). Animal death in both scaffold groups occurred within the first 9 d post-op and post-mortem analysis revealed esophageal obstruction due to fur ingestion in three rats receiving SF grafts and one animal implanted with SIS. Peritonitis with intra-peritoneal abscess was also confirmed in one rat grafted with SIS with the probable cause of death attributed to matrix rupture. No clinical signs of esophageal dysphasia or excessive salivation were observed in the surviving rats from any experimental group over the duration of the study period.

Gross tissue evaluations at 2 m post-op demonstrated extensive host tissue ingrowth spanning the entire area of the original implantation site in animals grafted with SF and SIS scaffolds (Figure 1C, D). External esophageal cysts were found attached to the implantation site in 15% (3/20) of animals receiving SIS grafts, while no cysts were observed in SF and

sham control groups. In addition, longitudinal contraction of the initial scaffold integration site was noted between the proximal/distal marking sutures in 50% (10/20) of the SIS cohort in comparison to 10% (2/20) of the SF group. Furthermore, the extent of longitudinal contraction encountered in the SIS group resulted in a 43–79% reduction in the length of the original implantation site, in comparison to 11–21% observed in the SF group. These observations demonstrate that SF matrices are superior in their ability to reinforce esophageal implantation sites in comparison to SIS scaffolds. The propensity of biomaterials to maintain the mechanical integrity of graft sites during host tissue integration is essential to maximize the extent of defect consolidation [41].

Tensile testing (Figure 2) revealed that the consolidated tissues supported by SF and SIS scaffolds displayed mean UTS values corresponding to 22% and 41% of sham levels, respectively. In addition, de novo tissues in SF and SIS groups exhibited respective mean ETF values which were 114% and 101% of sham values. Mean EM measurements were found to be significantly different between the experimental groups. The SF cohort displayed 56% of sham levels while the SIS group demonstrated a significant increase in EM corresponding to 531% of esophagotomy controls, indicating an elevation in tissue stiffness. Previous studies have correlated enhanced esophageal tissue stiffness with higher rates of organ dysmotility [42], therefore raising concerns over the long-term functional performance of SIS implants.

Animals in each experimental group were capable of solid food consumption following a 3 d post-op liquid diet and demonstrated similar degrees of weight gain throughout the study period (Figure 3). End-point μCT analysis of both scaffold groups at 2 m following implantation revealed preservation of organ continuity similar to sham control features with no evidence of contrast extravasation, fistulas, or diverticula (Figure 4A). In addition, no significant differences were observed between the luminal esophageal cross-sectional areas at the original surgical site or at the T7 level in any of the implant groups (Figure 4B), thus confirming the lack of strictures and organ dilatation.

Esophageal peristalsis is a sequentially coordinated mechanism which involves propagation of ingested food bolus distally toward the stomach via radially symmetrical contraction and relaxation of circular muscle [43]. In order to assess the potential of reconstructed esophageal segments to participate in this process, functional assessments of contractile and relaxation behaviors in experimental groups were evaluated at 2 m post-implantation. Contractile responses to nerve stimulation following EFS were observed in a frequency-dependent manner in circular esophageal rings isolated from both scaffold cohorts. These responses were not different from sham controls, indicating sufficient recovery of functional innervation in the repaired esophageal conduit (Figure 5A). Induction of muscle contractility by KCl-mediated membrane depolarization demonstrated that both implant groups were capable of generating ~50% of tensile force encountered in sham controls, indicating the integrity of the contractile apparatus in reconstructed conduits (Figure 5B). In addition, similar degrees of relaxation responses were observed in carbachol-stimulated tissue rings from both SF and SIS groups following isoproterenol administration (Figure 5C). Collectively, these data show that reconstructed esophageal conduits supported by both scaffold groups exhibited contractile and relaxation properties in a rat defect model.

Constructive tissue remodeling and host tissue responses elicited by SF scaffolds were characterized over the course of the study period and compared to SIS grafts and sham-operated controls at 2 m post-op by global histological (MTS, H&E) analyses (Figure 6). Following 1 d post-implantation, neutrophils and mononuclear inflammatory cells were found throughout the graft site supported by SF biomaterials with initial fragmentation of the porous scaffold compartment observed. At 1 wk post-op, vascularized, connective tissue ingrowth from the native esophageal wall traversed the entire SF graft site. The consolidated tissue was populated with fibroblasts and mononuclear inflammatory cells and was lined by a stratified squamous, keratinized epithelium which displayed comparable morphological features observed in sham-operated controls. Integration of nascent skeletal muscle fibers and smooth muscle bundles extending respectively from the host muscularis externa and muscularis mucosa were concentrated along the boundaries of the initial anastomosis. Scaffold remnants were scattered throughout the de novo esophageal wall and surrounded by focal points of putative macrophage phagocytosis. In some cases, residual luminal fragments of the bi-layer SF matrices were also present.

By 1 m post-op, an ECM-rich lamina propria was evident throughout the SF graft area with areas of mild fibrosis localized within the central portion of the consolidated tissue. The de novo muscularis mucosa extended further into the implant region in comparison to 1 wk timepoint, however this compartment transitioned into a discontinuous patchwork of smooth muscle bundles toward the center of the neotissue. The architecture of the de novo muscularis externa demonstrated increased organization into inner circular and outer longitudinal skeletal muscle layers along the periphery of the de novo esophageal wall, while smaller skeletal muscle bundles intercalated with mononuclear inflammatory cells spanned the interior of the original graft site. Degradation of the SF scaffolds was more pronounced at this timepoint with only scant residual fragments detected within the regenerating esophageal wall.

At 2 m post-implantation, the density of skeletal muscle within the muscularis externa present within the central region of the SF graft site was qualitatively increased in comparison to 1 m levels and individual layers displayed circular and longitudinal organization similar to peripheral areas. The de novo muscularis mucosa was underdeveloped relative to sham-operated controls. However, disjointed foci of smooth muscle bundles were observed throughout the interior of the implantation site to a qualitatively greater extent than seen in the 1 m timepoint. In addition, the architecture of the de novo epithelium in consolidated tissues at 1 and 2 m post-op was qualitatively similar to the 1 wk timepoint and sham-operated controls. Areas of mild fibrosis persisted within the interior of the consolidated tissue at this stage of regeneration, however chronic inflammatory reactions were not observed. Residual SF scaffold fragments were also undetectable in the majority of animals.

Parallel histological analyses of animals grafted with SIS matrices following 2 m of implantation demonstrated the formation of a de novo esophageal wall spanning the entire circumference of the graft area. Cross-sectional organization of the consolidated tissue consisted of a vascularized, lamina propria lined by a luminal, stratified squamous, keratinized epithelium similar in morphology to that observed in the other experimental

groups. In contrast to the SF cohort, host ingrowth of the muscularis externa was primarily restricted to the periphery of the graft site and consisted of disorganized skeletal muscle bundles. In addition, host integration of the muscularis mucosa was also confined to the exterior boundaries of the neotissue. Chronic inflammatory reactions were also elicited by the SIS grafts with foreign body responses characterized by multi-nuclear giant cells encapsulating residual scaffold remnants observed. Furthermore, mobilized follicular aggregates of mononuclear inflammatory cells as well as areas of severe fibrosis were predominant throughout the consolidated tissues. Tissue fibrosis is known to contribute to increased levels of tissue stiffness [44] and therefore higher extents of fibrotic tissue remodeling in SIS graft sites may explain the elevation in elastic modulus observed in comparison to the other experimental groups where fibrosis was minimal. Overall, our results demonstrate that SF grafts are less immunogenic, and promote greater extents of constructive tissue remodeling in comparison to SIS implants during esophageal repair.

Previous reports have shown that homeostasis of the rodent esophageal epithelium is maintained by a population of proliferative basal cells which, on commitment to terminal differentiation, exit the cell cycle and subsequently migrate to the tissue surface and undergo exfoliation [45]. This basal cell population divides stochastically to generate proliferating and differentiating daughter cells with equal probability [45]. In response to surface wounds, basal cells reversibly switch to produce an excess of proliferating daughter cells which migrate into the defect site [45]. Once wound closure has been achieved, the infiltrating basal progenitor population reduce their rate of proliferation to baseline levels and undergo differentiation to reconstitute the native epithelial layers [45]. In contrast to intestinal epithelia [46], this fate switching behavior enables a single progenitor basal population to both maintain and repair tissue without the need for a slow-cycling stem cell pool which is absent in the rodent esophagus [45].

IHC and histomorphometric analyses were performed on host and de novo epithelia to characterize the stages of regeneration and extent of maturation achieved in experimental groups (Figure 7). In contrast to previous models of mucosal damage [45], the phases of epithelial regeneration in full thickness defects following biomaterial implantation have been poorly studied. Prior to surgical manipulation, IHC evaluations of the host stratified squamous, keratinized epithelium revealed a basal cell compartment lining the lamina propria which consisted of 1–2 layers of cells with a cuboidal morphology expressing robust levels of CK5. Nuclear Ki67 expression was confirmed in 31±9% of the basal cell population, indicative of cell proliferation. Suprabasal cells displaying a polygonal morphology, large nuclei, and sparse CK5 expression level were organized into 1–2 cell layers overlying the basal cell zone. The external superficial cell layers contained elliptical nuclei and a progressively flattened cellular morphology with the outermost apical layers transitioning to keratinized squames positive for IVL expression. Following 1 d after grafting with SF matrices, the host epithelium adjacent to the site of anastomosis underwent exfoliation of the luminal superficial cell layers. CK5 expression was qualitatively upregulated in the suprabasal compartment and nuclear Ki67 expression was now evident in 59±11% of the basal cell layer. The increase in basal cell proliferation in the host epithelial regions surrounding the scaffold implantation site was comparable to the responses previously reported following mucosal damage [45].

By 1 wk post-op, a stratified squamous, keratinized epithelium had formed throughout the SF implant site. The de novo epithelium consisted of 1–2 layers of basal cells with 22±17% of this population demonstrating nuclear Ki67 positivity. In contrast to nonsurgical controls, 4–8 layers of polygonal, suprabasal cells were observed within the graft site which were lined by 2–3 layers of flattened superficial cells displaying punctate IVL protein expression. Both the suprabasal and superficial cell compartments exhibited prominent CK5 expression which persisted throughout the 2 m SF implantation period. Although the origin of the epithelial progenitor cell population responsible for reconstitution of the implant site is unknown, the proliferating basal cell compartment present in adjacent host tissues is a likely candidate, however future lineage tracing experiments are needed to confirm this notion.

Normalization of suprabasal cell hyperplasia to 1–2 layers was evident by 2 m post-op within the SF graft site, however IVL protein expression in the superficial cell layers displayed a similar pattern as observed at the 1 wk timepoint. The de novo epithelia present at the site of SIS implantation as well as in sham-operated controls following 2 m post-op displayed comparable morphological and CK5 and IVL expression patterns as demonstrated by the SF cohort. In addition, histomorphometric analysis revealed similar extents of pan-CK+ epithelia across both implant groups and sham-operated controls at each timepoint examined. Fundamental differences in CK5 and IVL expression patterns observed throughout all experimental groups at 2 m post-op in comparison to nonsurgical controls may reflect incomplete maturation of reconstituted epithelia. Future experiments will focus on longer implantation times to ascertain the ability of the de novo epithelia to acquire a baseline phenotype.

IHC evaluations demonstrated the formation of MY32+ skeletal muscle bundles and α-SMA + smooth muscle bundles (Figure 8) within the periphery of the SF graft area following 1 wk of implantation, indicative of contractile differentiation. The percent of MY32+ area supported by SF implants significantly increased in the regenerating muscularis externa at 2 m post-op in comparison to the early timepoints and was found to be similar to the levels achieved in sham-operated controls. In contrast, the extent of MY32+ skeletal muscle bundles at sites of SIS implantation following 2 m post-op was significantly lower in respect to both sham-operated controls and the SF group. Over the course of 1 m of SF matrix implantation, the amount of α-SMA+ muscularis mucosa increased by 3.4-fold over 1 wk baseline levels in the de novo esophageal tissue and eventually plateaued at 2 m to a similar extent as observed in sham-operated controls. In contrast, consolidated tissues present in the SIS group achieved only 41% of the α-SMA+ area observed in sham-operated controls.

Regenerated tissues supported by both SF and SIS matrices displayed evidence of *de novo* innervation throughout the original implantation sites characterized by the appearance of SYP38+ boutons indicative of areas of synaptic transmission (Figure 9). Following 1 m of SF matrix grafting, histomorphometric analysis demonstrated a significant 3.2-fold increase in the density of SYP38+ boutons present at the 1 wk timepoint. This level had plateaued by 2 m post-op and was found to be similar to extent of innervation displayed by sham-operated controls. In contrast, the density of SYP38+ boutons observed in the neotissues supported by the SIS cohort was significantly lower in comparison to the other experimental groups at similar timepoints and constituted only 29% of sham-operated control levels.

Vessels containing CD31+ endothelial cells were present throughout the consolidated tissues in both implant groups and sham-operated controls at each timepoint examined (Figure 9). Histomorphometric evaluations revealed that the vascularization pattern in the neotissues was differentially affected by implantation time as well as the type of biomaterial utilized for tissue repair. In particular, a significant decline in vessel density was observed within the SF graft sites at 2 m postop in comparison to 1 wk levels. These results are consistent with data from other wound healing models wherein vessel density declines as tissue maturation proceeds and new ECM is deposited [47]. In addition, evaluation of vessel density following 2 m of implantation revealed that the SIS group displayed significantly higher levels of this parameter in respect to the extent achieved in all other cohorts; a feature which may reflect the immature state of the neotissue supported by this matrix configuration [47]. In contrast, no significant differences in mean vessel diameter were noted at various temporal stages of tissue remodeling examined in the SF groups or between any of the experimental groups at the 2 m timepoint (data not shown).

4. Conclusions

In the present study, we demonstrate the feasibility of bi-layer SF scaffolds to serve as acellular grafts for esophageal tissue repair in a rat model. These biomaterials supported consolidation of semi-circumferential defects and promoted the formation of innervated, vascularized epithelial and muscular tissues. In addition, SF grafts were capable of maintaining organ continuity and supporting solid food consumption. In comparison to conventional SIS implants, SF matrices displayed reductions in graft site contracture, elicited minimal inflammatory reactions and fibrosis, and promoted significantly higher degrees of skeletal muscle and innervation within implantation sites. In summary, bi-layer SF grafts offer promising platforms for esophageal tissue engineering.

Acknowledgments

This research was supported by the Tissue Engineering Resource Center, NIH/NIBIB P41 EB002520 (KAPLAN). This research was also supported through the vision and generosity of the Rainmaker Group in honor of Alan Retik, MD. We also acknowledge Dr. Rosalyn Adam for helpful discussions.

References

1. Shen KR, Austen WG Jr, Mathisen DJ. Use of a prefabricated pectoralis major muscle flap and pedicled jejunal interposition graft for salvage esophageal reconstruction after failed gastric pull-up and colon interposition. J Thorac Cardiovasc Surg. 2008; 135:1186–7. [PubMed: 18455610]
2. Burgos L, Barrena S, Andrés AM, Martínez L, Hernández F, Olivares P, et al. Colonic interposition for esophageal replacement in children remains a good choice: 33-year median follow-up of 65 patients. J Pediatr Surg. 2010; 45:341–5. [PubMed: 20152348]
3. Leonard GD, McCaffrey JA, Maher M. Optimal therapy for oesophageal cancer. Cancer Treat Rev. 2003; 29:275–82. [PubMed: 12927567]
4. Greene CL, DeMeester SR, Worrell SG, Oh DS, Hagen JA, DeMeester TR. Alimentary satisfaction, gastrointestinal symptoms, and quality of life 10 or more years after esophagectomy with gastric pull-up. J Thorac Cardiovasc Surg. 2014; 147:909–14. [PubMed: 24332098]
5. Romeo C, Bonanno N, Baldari S, Centorrino A, Scalfari G, Antonuccio P, et al. Gastric motility disorders in patients operated on for esophageal atresia and tracheoesophageal fistula: long term evaluation. J Pediatr Surg. 2000; 35:740–4. [PubMed: 10813339]

6. Deurloo JA, Ekkelkamp S, Hartman EE, Sprangers MA, Aronson DC. Quality of life in adult survivors of correction of oesophageal atresia. Arch Surg. 2005; 140:976–80. [PubMed: 16230548]
7. Somppi E, Tammela O, Ruuska T, Rahnasto J, Laitinen J, Turjanmaa V, et al. Outcome of patients operated on for oesophageal atresia: 30 years' experience. J Pediatr Surg. 1998; 33:1341–6. [PubMed: 9766349]
8. Tan JY, Chua CK, Leong KF, Chian KS, Leong WS, Tan LP. Esophageal tissue engineering: an in-depth review on scaffold design. Biotechnol Bioeng. 2012; 109:1–15. [PubMed: 21915849]
9. Totonelli G, Maghsoudlou P, Fishman JM, Orlando G, Ansari T, Sibbons P, et al. Esophageal tissue engineering: a new approach for esophageal replacement. World J Gastroenterol. 2012; 18:6900–7. [PubMed: 23322987]
10. Levin DE, Grikscheit TC. Tissue-engineering of the gastrointestinal tract. Curr Opin Pediatr. 2012; 24:365–70. [PubMed: 22450251]
11. Del Gaudio C, Baiguera S, Ajalloueian F, Bianco A, Macchiarini P. Are synthetic scaffolds suitable for the development of clinical tissue-engineered tubular organs? J Biomed Mater Res A. 2014; 102:2427–47. [PubMed: 23894109]
12. Bhrany AD, Beckstead BL, Lang TC, Farwell DG, Giachelli CM, Ratner BD. Development of an esophagus acellular matrix tissue scaffold. Tissue Eng. 2006; 12:319–30. [PubMed: 16548690]
13. Badylak S, Meurling S, Chen M, Spievack A, Simmons-Byrd A. Resorbable bioscaffold for esophageal repair in a dog model. J Pediatr Surg. 2000; 35:1097–103. [PubMed: 10917304]
14. Isch JA, Engum SA, Ruble CA, Davis MM, Grosfeld JL. Patch esophagoplasty using AlloDermas a tissue scaffold. J Pediatric Surg. 2001; 36:266–8.
15. Urita Y, Komuro H, Chen G, Shinya M, Kaneko S, Kaneko M, et al. Regeneration of the esophagus using gastric acellular matrix: an experimental study in a rat model. Pediatr Surg Int. 2007; 23:21–6. [PubMed: 17004093]
16. Lopes MF, Cabrita A, Ilharco J, Pessa P, Paiva-Carvalho J, Pires A, et al. Esophageal replacement in rat using porcine intestinal submucosa as a patch or a tube-shaped graft. Dis Esophagus. 2006; 19:254–9. [PubMed: 16866856]
17. Lopes MF, Cabrita A, Ilharco J, Pessa P, Patrício J. Grafts of porcine intestinal submucosa for repair of cervical and abdominal esophageal defects in the rat. J Invest Surg. 2006; 19:105–11. [PubMed: 16531368]
18. Jönsson L, Gatzinsky V, Jennische E, Johansson C, Nannmark U, Friberg LG. Piglet model for studying esophageal regrowth after resection and interposition of a silicone stented small intestinal submucosa tube. Eur Surg Res. 2011; 46:169–79. [PubMed: 21454984]
19. Tan B, Wang M, Chen X, Hou J, Chen X, Wang Y, et al. Tissue engineered esophagus by copper--small intestinal submucosa graft for esophageal repair in a canine model. Sci China Life Sci. 2014; 57:248–55. [PubMed: 24443178]
20. Kajitani M, Wadia Y, Hinds MT, Teach J, Swartz KR, Gregory KW. Successful repair of esophageal injury using an elastin based biomaterial patch. ASAIO J. 2001; 47:342–5. [PubMed: 11482483]
21. Takimoto Y, Okumura N, Nakamura T, Natsume T, Shimizu Y. Long-term follow-up of the experimental replacement of the esophagus with a collagen-silicone composite tube. ASAIO J. 1993; 39:M736–9. [PubMed: 8268635]
22. Takimoto Y, Nakamura T, Yamamoto Y, Kiyotani T, Teramachi M, Shimizu Y. The experimental replacement of a cervical esophageal segment with an artificial prosthesis with the use of collagen matrix and a silicone stent. J Thorac Cardiovasc Surg. 1998; 116:98–106. [PubMed: 9671903]
23. Yamamoto Y, Nakamura T, Shimizu Y, Matsumoto K, Takimoto Y, Kiyotani T, et al. Intrathoracic esophageal replacement in the dog with the use of an artificial esophagus composed of a collagen sponge with a double-layered silicone tube. J Thorac Cardiovasc Surg. 1999; 118:276–86. [PubMed: 10425001]
24. Yamamoto Y, Nakamura T, Shimizu Y, Matsumoto K, Takimoto Y, Liu Y, et al. Intrathoracic esophageal replacement with a collagen sponge--silicone double layer tube: evaluation of omental-pedicle wrapping and prolonged placement of an inner stent. ASAIO J. 2000; 46:734–9. [PubMed: 11110272]

25. Clough A, Ball J, Smith GS, Leibman S. Porcine small intestine submucosa matrix (Surgisis) for esophageal perforation. Ann Thorac Surg. 2011; 91:e15–6. [PubMed: 21256256]
26. Badylak SF, Hoppo T, Nieponice A, Gilbert TW, Davison JM, Jobe BA. Esophageal preservation in five male patients after endoscopic inner-layer circumferential resection in the setting of superficial cancer: a regenerative medicine approach with a biologic scaffold. Tissue Eng Part A. 2011; 17:1643–50. [PubMed: 21306292]
27. Nieponice A, Ciotola FF, Nachman F, Jobe BA, Hoppo T, Londono R, et al. Patch Esophagoplasty: Esophageal Reconstruction Using Biologic Scaffolds. Ann Thorac Surg. 2014; 97:283–8. [PubMed: 24266951]
28. Doede T, Bondartschuk M, Joerck C, Schulze E, Goernig M. Unsuccessful alloplastic esophageal replacement with porcine small intestinal submucosa. Artif Organs. 2009; 33:328–33. [PubMed: 19335409]
29. Aikawa M, Miyazawa M, Okamoto K, Okada K, Akimoto N, Sato H, et al. A bioabsorbable polymer patch for the treatment of esophageal defect in a porcine model. J Gastroenterol. 2013; 48:822–9. [PubMed: 23229769]
30. Grikscheit T, Ochoa ER, Srinivasan A, Gaissert H, Vacanti JP. Tissue-engineered esophagus: experimental substitution by onlay patch or interposition. J Thorac Cardiovasc Surg. 2003; 126:537–44. [PubMed: 12928655]
31. Nakase Y, Nakamura T, Kin S, Nakashima S, Yoshikawa T, Kuriu Y, et al. Intrathoracic esophageal replacement by in situ tissue-engineered esophagus. J Thorac Cardiovasc Surg. 2008; 136:850–9. [PubMed: 18954622]
32. Ceonzo K, Gaynor A, Shaffer L, Kojima K, Vacanti CA, Stahl GL. Polyglycolic acid-induced inflammation: role of hydrolysis and resulting complement activation. Tissue Eng. 2006; 12:301–8. [PubMed: 16548688]
33. Mauney JR, Cannon GM, Lovett ML, Gong EM, Di Vizio D, Gomez P 3rd, et al. Evaluation of gel spun silk-based biomaterials in a murine model of bladder augmentation. Biomaterials. 2011; 32:808–18. [PubMed: 20951426]
34. Seth A, Chung YG, Gil ES, Tu D, Franck D, Di Vizio D, et al. The performance of silk scaffolds in a rat model of augmentation cystoplasty. Biomaterials. 2013; 34:4758–65. [PubMed: 23545287]
35. Tu DD, Chung YG, Gil ES, Seth A, Franck D, Cristofaro V, et al. Bladder tissue regeneration using acellular bi-layer silk scaffolds in a large animal model of augmentation cystoplasty. Biomaterials. 2013; 34:8681–9. [PubMed: 23953839]
36. Franck D, Chung YG, Coburn J, Kaplan DL, Estrada CR Jr, Mauney JR. In vitro evaluation of bi-layer silk fibroin scaffolds for gastrointestinal tissue engineering. J Tissue Eng. 2014; 5:2041731414556849. [PubMed: 25396043]
37. Chung YG, Algarrahi K, Franck D, Tu DD, Adam RM, Kaplan DL, et al. The use of bi-layer silk fibroin scaffolds and small intestinal submucosa matrices to support bladder tissue regeneration in a rat model of spinal cord injury. Biomaterials. 2014; 35:7452–9. [PubMed: 24917031]
38. Chung YG, Tu D, Franck D, Gil ES, Algarrahi K, Adam RM, et al. Acellular bi-layer silk fibroin scaffolds support tissue regeneration in a rabbit model of onlay urethroplasty. PLoS One. 2014; 9:e91592. [PubMed: 24632740]
39. Kim UJ, Park J, Kim HJ, Wada M, Kaplan DL. Three-dimensional aqueous-derived biomaterial scaffolds from silk fibroin. Biomaterials. 2005; 26:2775–85. [PubMed: 15585282]
40. Pang J, Borjeson TM, Muthupalani S, Ducore RM, Carr CA, Feng Y, et al. Megaesophagus in a Line of Transgenic Rats: A Model of Achalasia. Vet Pathol. 2014; 51:1187–200. [PubMed: 24457157]
41. Lee M, Chang PC, Dunn JC. Evaluation of small intestinal submucosa as scaffolds for intestinal tissue engineering. J Surg Res. 2008; 147:168–71. [PubMed: 18406427]
42. Zeng YJ, Yang J, Zhao JB, Liao DH, Zhang EP, Gregersen H, et al. Morphologic and biomechanical changes of rat oesophagus in experimental diabetes. World J Gastroenterol. 2004; 10:2519–23. [PubMed: 15300896]
43. Paterson, WG. Esophageal peristalsis. In: Goyal, R.; Shaker, R., editors. Part 1 Oral cavity, pharynx and esophagus. GI Motility Online 2006.

44. Cox TR, Erler JT. Remodeling and homeostasis of the extracellular matrix: implications for fibrotic diseases and cancer. Dis Model Mech. 2011; 4:165–78. [PubMed: 21324931]

45. Doupé DP, Alcolea MP, Roshan A, Zhang G, Klein AM, et al. A single progenitor population switches behavior to maintain and repair esophageal epithelium. Science. 2012; 337:1091–3. [PubMed: 22821983]

46. Barker N, van Es JH, Kuipers J, Kujala P, van den Born M, et al. Identification of stem cells in small intestine and colon by marker gene Lgr5. Nature. 2007; 449:1003–7. [PubMed: 17934449]

47. Tonnesen MG, Feng X, Clark RA. Angiogenesis in wound healing. J Investig Dermatol Symp Proc. 2000; 5:40–6.

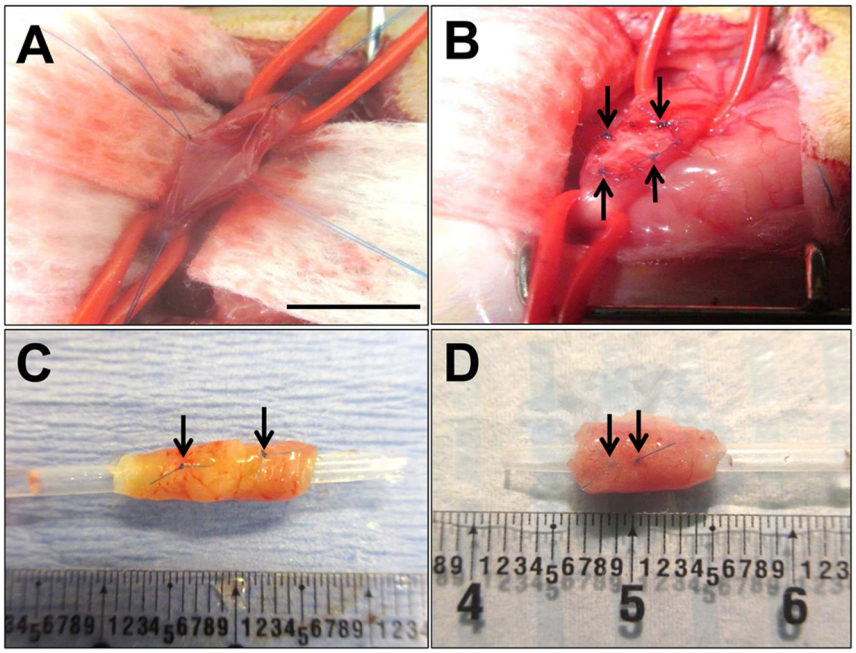

Figure 1. Rat onlay esophagoplasty model

Photomicrographs of various surgical stages of scaffold implantation and gross morphology of regenerated tissues. [**A**] Esophagotomy and exposure of the esophagus lumen. [**B**] Anastomosis of bi-layer silk fibroin (SF) graft into the esophagus defect. [**C**, **D**] Regenerated tissues present within the original implantation sites supported by SF scaffolds [C] and small intestinal submucosa (SIS) matrices [D] at 2 m post-op. Arrows denote original marking sutures. Scale bars = 7 mm.

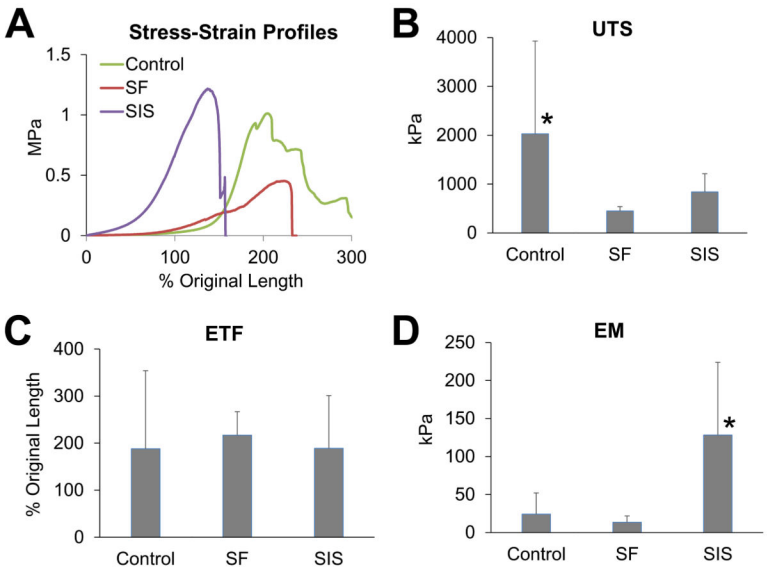

Figure 2. Tensile properties of regenerated esophageal tissues supported by implant and sham control groups

[**A**] Representative stress-strain profiles of experimental groups at 2 m post-op. [**B**–**D**] Evaluation of ultimate tensile strength (UTS), elongation to failure (ETF), and elastic modulus (EM) in cohorts defined in [A]. Means ± standard deviation per data point. (*) = $p<0.05$ in comparison to all other groups.

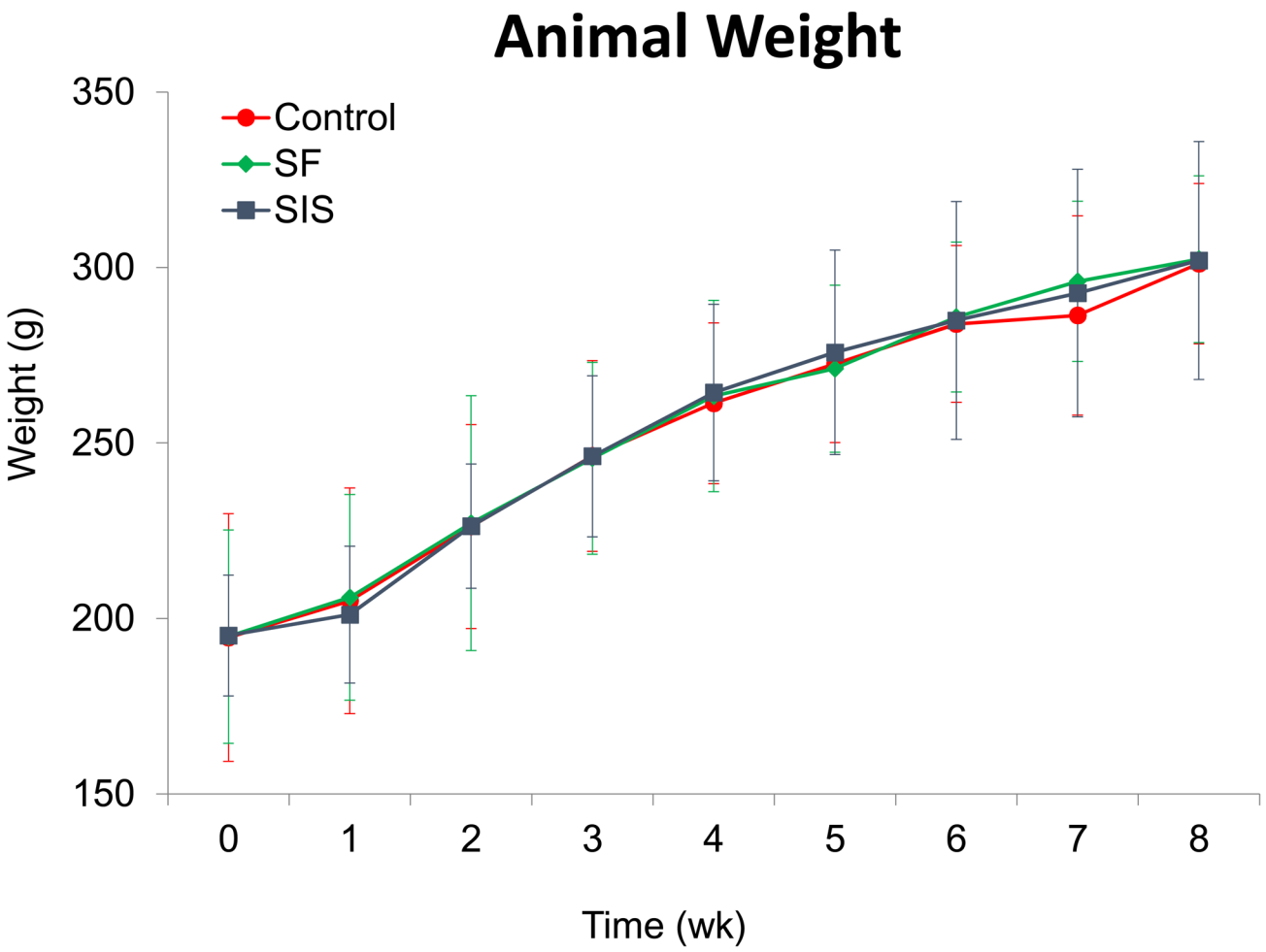

Figure 3. Body weight evaluations in matrix-grafted animals and sham controls both pre-operatively and over the course of the study period

All experimental subjects were fed a liquid diet for 3 d post-op and subsequently maintained on solid food thereafter. Means ± standard deviation per data point.

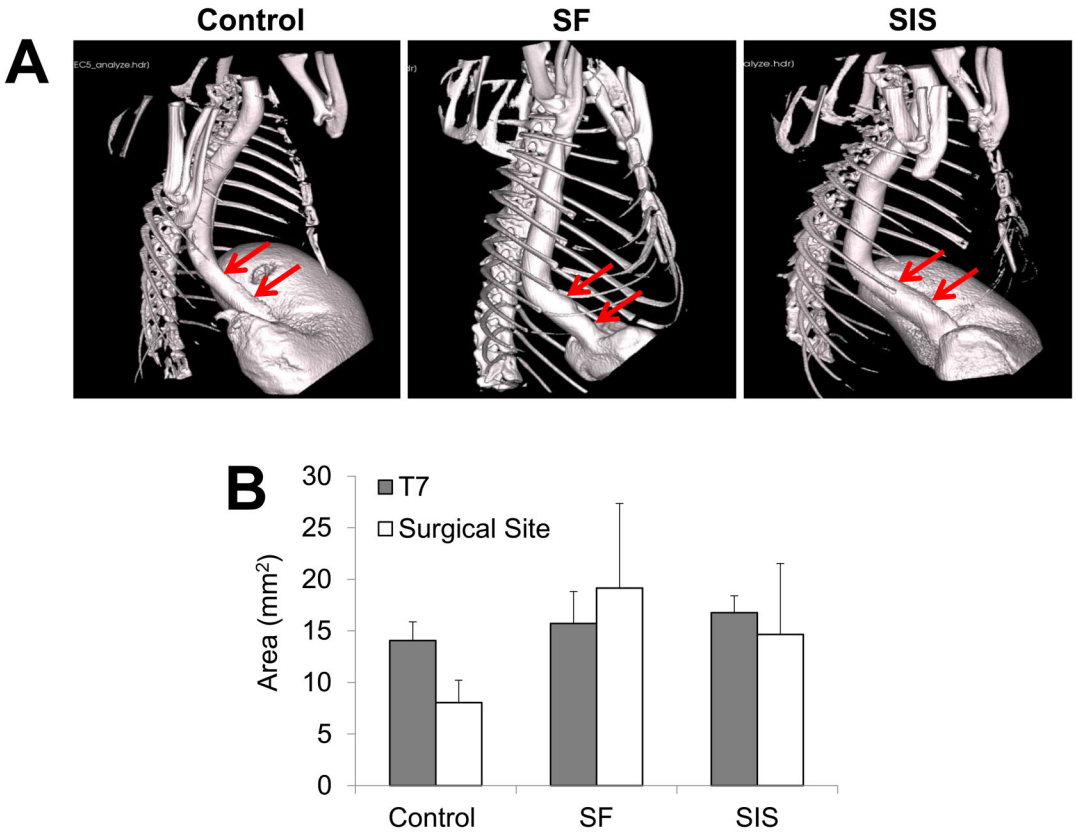

Figure 4. μCT analysis of esophageal continuity in implant and sham control groups

[**A**] Representative 3-D images of esophagi in experimental groups at 2 m post-op following contrast gavage. Arrows denote boundaries of original graft anastomosis or esophagotomy in controls. [**B**] Quantification of luminal esophageal cross-sectional areas from the central region of the original scaffold anastomosis or esophagotomy in controls (surgical sites) as well as a nonsurgical reference point adjacent to the 7th thoracic vertebra (T7). Means ± standard deviation per data point.

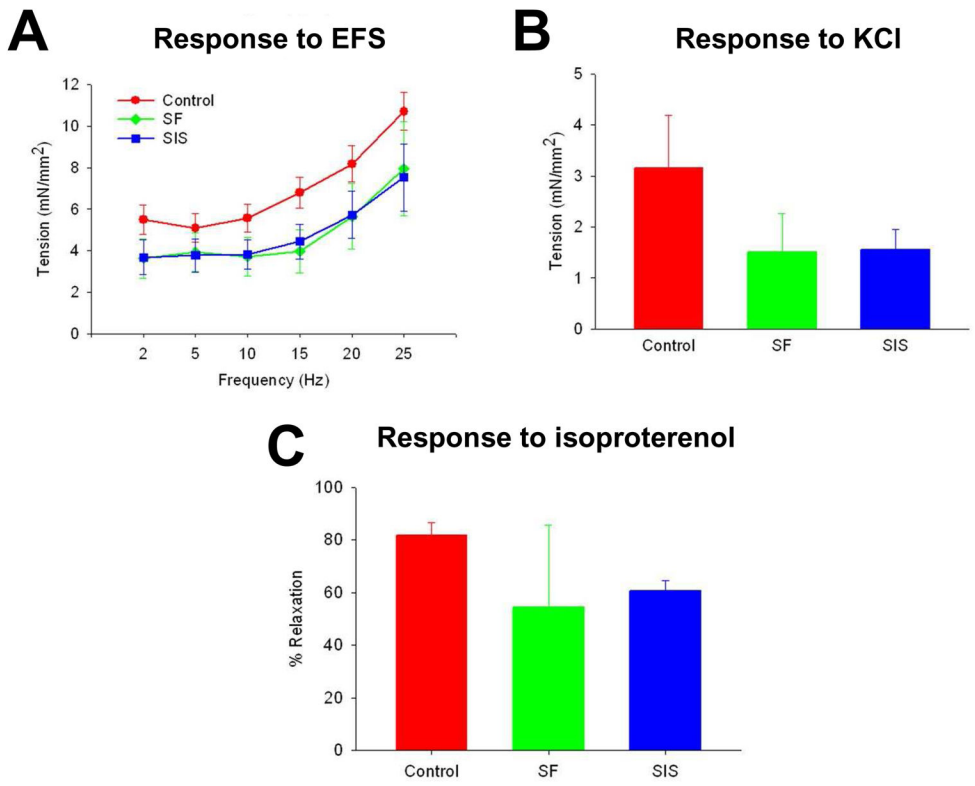

Figure 5. Ex vivo tissue contractility and relaxation responses in reconstructed esophageal conduits isolated from matrix and sham control groups

[**A**] Frequency response curves to electrical field stimulation (EFS) in circular esophageal rings containing original graft sites or esophagotomy region following 2 m post-op. [**B**] Contractile responses to KCl (80 mM) in specimens described in [A]. [**C**] Relaxation responses in samples detailed in [A] in response to isoproterenol (10 μM) following pre-contraction with carbachol (1 μM). Means ± standard deviation per data point.

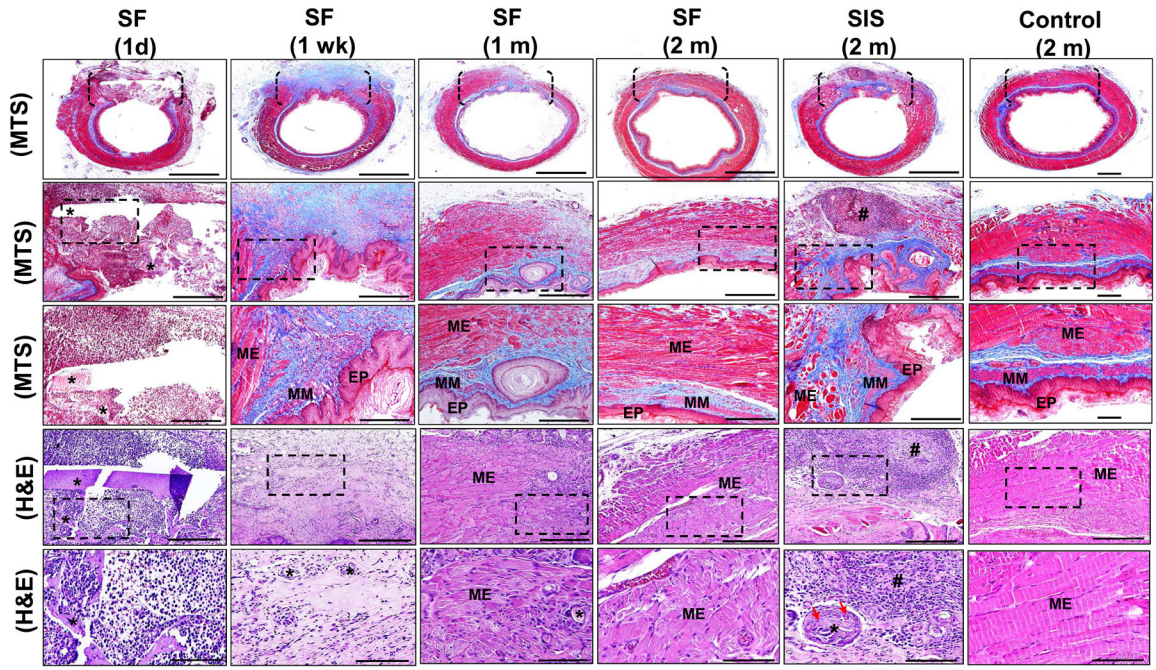

Figure 6. Histological evaluations of tissue regeneration and host responses in sham controls and implant groups

[**1st row**] Photomicrographs of MTS-stained gross esophageal cross-sections containing region of tissue repair. Brackets denote sites of scaffold anastomosis or control esophagotomy. Scale bars = 1.25 mm. [**2nd row**] Magnification of global tissue regeneration area (RA) bracketed in 1st column. Scale bars = 750 μm. [**3rd row**] Magnified boxed area in 2nd column. Scale bars = 250 μm. [**4th row**] Photomicrographs of H&E-stained sections from bracketed area described in 1st column. Scale bars = 250 μm. [**5th row**] Magnified boxed area in 4th row. Scale bars = 80 μm. EP = epithelium; MM = muscularis mucosa; ME = muscularis externa. (*) = scaffold remnants. (#) = aggregate of mononuclear cells indicative of chronic inflammation. Red arrows denote multi-nuclear giant cells encapsulating residual scaffold remnants.

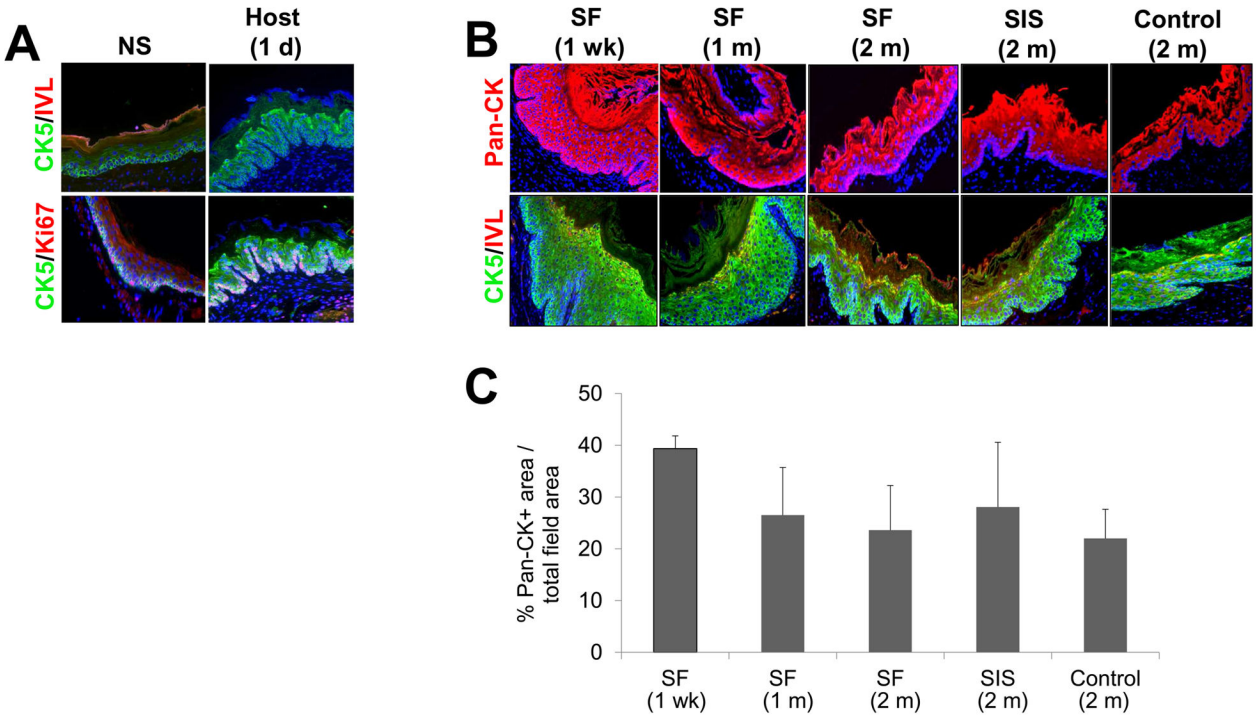

Figure 7. Immunohistochemical and histomorphometric assessments of epithelial regeneration in controls and scaffold groups

[**A**] Photomicrographs of involucrin (IVL), cytokeratin 5 (CK5), and Ki67 protein expression in epithelia present in nonsurgical (NS) controls and in host tissue adjacent to the site of SF scaffold anastomosis. [**B**] Photomicrographs of pan-CK, IVL, and CK5 protein expression in de novo epithelia present within the original graft sites or control esophagotomy area. For all panels, respective marker expression is displayed in red (Cy3) or green (FITC) labeling. Blue denotes DAPI nuclear counterstain. Scale bars in all panels = 200 μm. [**C**] Histomorphometric analysis of the extent of pan-CK+ epithelia present at site of tissue repair in scaffold groups or sham-operated controls.

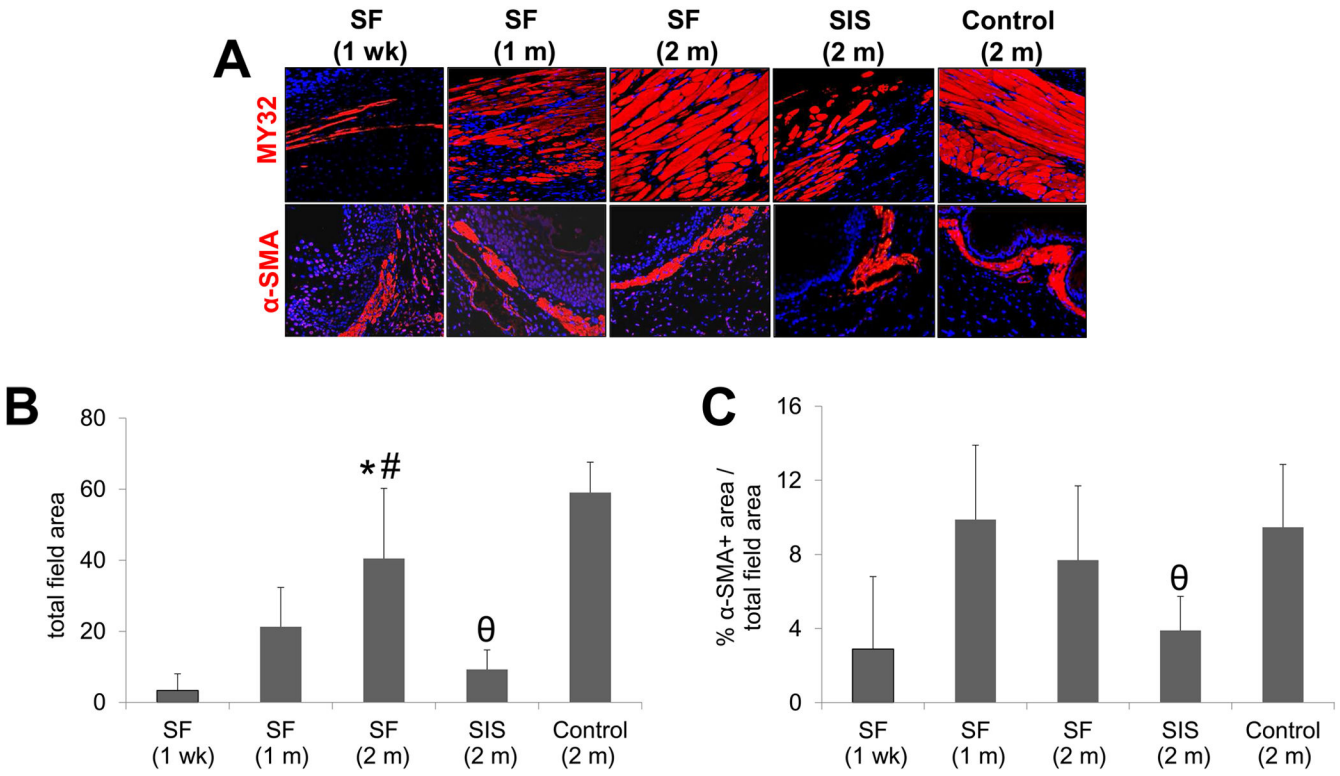

Figure 8. Immunohistochemical and histomorphometric evaluations of skeletal and smooth muscle formation in sham controls and scaffold groups

[**A**] Photomicrographs of fast myosin skeletal heavy chain (MY32) and α-smooth muscle actin (α-SMA) protein expression in de novo muscularis externa and muscularis muscosa, respectively, within the original graft site or control esophagotomy area. For all panels, respective marker expression is displayed in red (Cy3) labeling. Blue denotes DAPI nuclear counterstain. Scale bars in all panels = 200 μm. [**B**, **C**] Histomorphometric analysis of the extent of MY32+ skeletal muscle [B] and α-SMA+ smooth muscle [C] present at sites of tissue repair in matrix groups or sham controls. (*) = $p<0.05$ in comparison to both 1 wk and 1 m SF groups. (#) = $p<0.05$ in comparison to SIS. (θ) = $p<0.05$ in comparison to sham control.

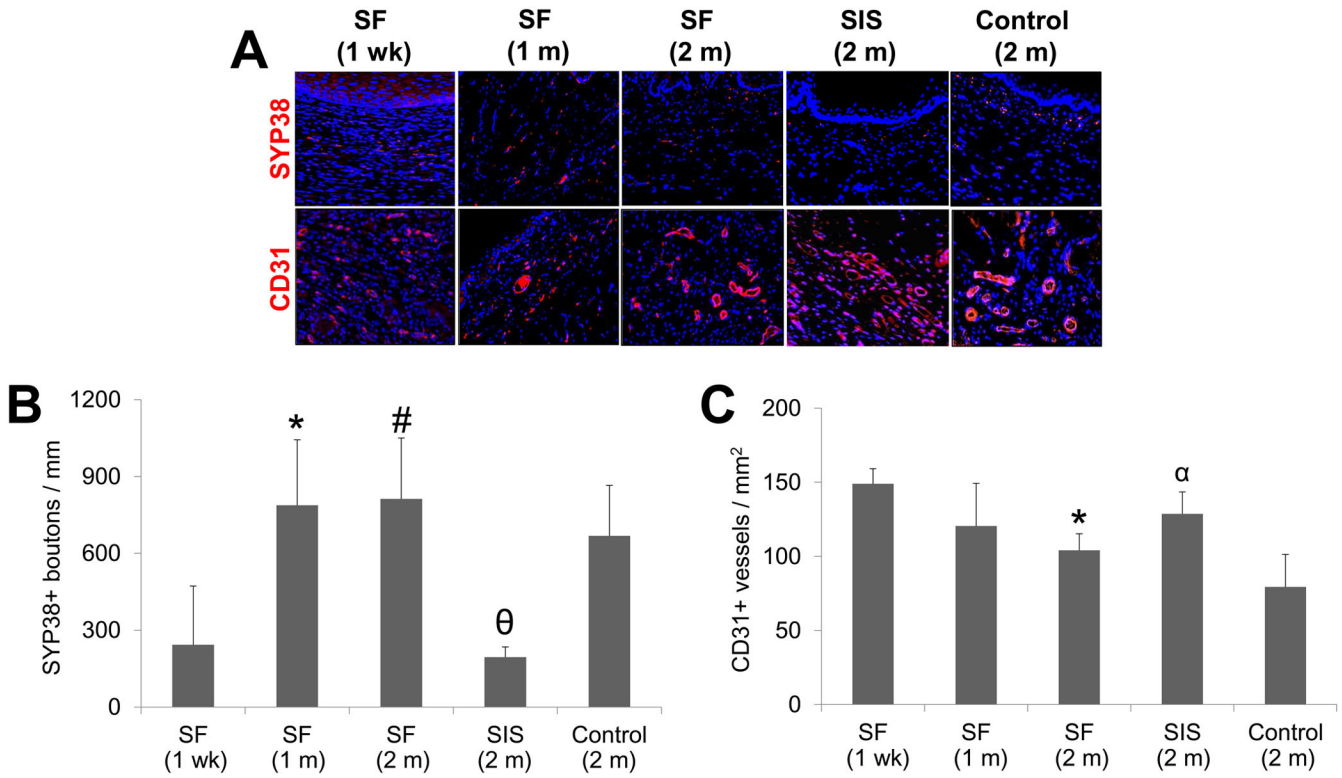

Figure 9. Immunohistochemical and histomorphometric analyses of de novo innervation and vascularization in experimental groups

[**A**] Photomicrographs of synaptophysin (SYP38) and CD31 protein expression present within original graft sites or control esophagotomy area. For all panels, respective marker expression is displayed in red (Cy3) labeling. Blue denotes DAPI nuclear counterstain. Arrows denote SYP38+ boutons. Scale bars in all panels = 200 μm. [**B**, **C**] Histomorphometric analysis of density of SYP38+ boutons [B] and CD31+ vessels [C] observed at sites of tissue regeneration in implant groups or sham controls. (*) = $p<0.05$ in comparison to 1 wk SF group. (#) = $p<0.05$ in comparison to SIS. (θ) = $p<0.05$ in comparison to sham control. (α) = $p<0.05$ in comparison to all other 2 m groups.